Scaling AlGaN/GaN High Electron Mobility Transistor Structures onto 200-mm Silicon (111) Substrates through Novel Buffer Layer Configurations

H.-P. Lee[1, 2], J. Perozek[1, 2], and C. Bayram* [1, 2]

[1]Department of Electrical and Computer Engineering, University of Illinois at Urbana-Champaign, Urbana, Illinois 61801, USA
[2]Micro and Nanotechnology Laboratory, University of Illinois at Urbana-Champaign, Urbana, Illinois 61801, USA
*e-mail: cbayram@illinois.edu

Keywords: AlGaN, Si, high electron mobility transistor, two-dimensional electron gas, defectivity, strain

Abstract

Crack-free and low-bow (< 50 µm) AlGaN/GaN high electron mobility transistor (HEMT) structures are grown on 200-mm diameter Si(111) substrates by using three different buffer layer configurations: (a) Thick-GaN / 3 × {$Al_xGa_{1-x}N$} / AlN, (b) Thin-GaN / 3 × {$Al_xGa_{1-x}N$} / AlN, and (c) Thin-GaN / AlN. Optical, structural, and electrical properties of these AlGaN/GaN HEMT structures are reported. The effects of buffer layer stacks (i.e. thickness and content) on defectivity, stress, and two-dimensional electron gas (2DEG) mobility and concentration are studied. We show that the in-plane stress type and magnitude significantly affect the 2DEG characteristic, suggesting the importance of optimal buffer layer configurations for AlGaN/GaN HEMTs on Si(111) substrates.

INTRODUCTION

AlGaN/GaN high electron mobility transistors (HEMTs) are being investigated for high power high frequency applications, as III-nitride (i.e. GaN) materials have high thermal and chemical stability, high breakdown field (> 3 MV/cm), and high electron saturation velocity (> 2.5 × 10^7 cm/s) [1]. As such, GaN-on-silicon (111) technology is driven by the need of reducing cost and integration with CMOS technology. For scaling beyond conventional 4-inch diameter substrates, Si is the key but scaling up to and beyond 200-mm diameter comes with further challenges in wafer bow (< 50µm) and cracking prevention. Given the lattice mismatch of ~17%, combined with the large thermal-expansion-coefficient mismatch of ~54% between GaN and Si(111), a novel (Al)GaN buffer layer configuration is required to minimize such mismatch-effects [2]. In addition, devices made on different wafer positions can also vary in electrical performance [3].

It is known that the performance of AlGaN/GaN HEMTs is governed by the two-dimensional electron gas (2DEG) properties, which forms at the AlGaN-GaN hetero-interface. Particularly, a high 2DEG density reduces source/drain channel resistance and increases the power output; in addition, a high 2DEG mobility enhances the AlGaN/GaN HEMTs high frequency performance. In this work, we grew identical AlGaN/GaN HEMT structures on 200-mm Si(111) substrates with three different buffer layer configurations and report the effects of buffer layer configurations on the AlGaN/GaN HEMT structure properties. We investigate these structures using optical microscopy, atomic-force microscopy (AFM), cathodoluminescence (CL), X-ray diffraction (XRD) reciprocal space mapping (RSM) and Hall measurements. We then correlate the electrical properties of AlGaN/GaN HEMT structures with the embodied buffer layer properties and report the effects of buffer layer stress and defectivity on the 2DEG concentration and mobility [4].

RESULT

Structures of the crack-free and low-bow (< 50 µm) MOCVD-grown AlGaN/GaN HEMT on 200-mm-diameter Si(111) substrate with three different buffer configurations are shown in Fig. 1: (a) Thick-GaN / 3 × {$Al_xGa_{1-x}N$} / AlN (Sample A, 6.3 µm epi thickness), (b) Thin-GaN / 3 × {$Al_xGa_{1-x}N$} / AlN (Sample B, 2.0 µm epi thickness), and (c) Thin-GaN / AlN (Sample C, 1.1 µm epi thickness). Atop of all samples (A, B, C), the same AlGaN/GaN HEMT structure, composed of 3-nm-thick i-GaN / 17-nm-thick $Al_xGa_{1-x}N$ / 1-nm-thick AlN, is deposited. CL spectroscopy with 1.5 kV electron acceleration voltage (yields 29-nm penetration depth) reveal the Al composition of the $Al_xGa_{1-x}N$ barrier layer to be 0.25, 0.23, and 0.22 for sample A, B, and C, respectively (Fig. 2). The inserted AlN spacer layer serves to increase the conduction band offset (better confinement) in order to increase the 2DEG concentration and mobility.

Fig. 1. AlGaN/GaN HEMT structure grown on 200-mm-diameter Si(111) with different buffer layer configurations.

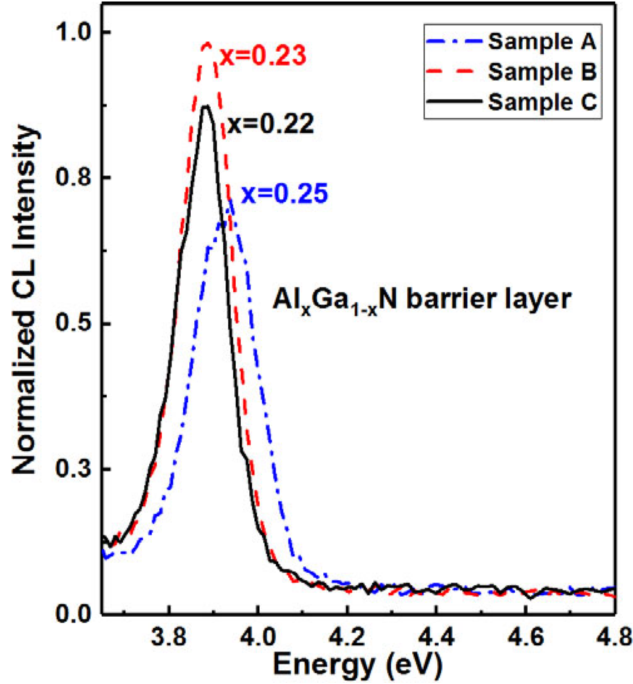

Fig. 2. Cathodoluminescence investigations using 1.5kV electron acceleration voltage, yielding a 29-nm penetration depth, reveals the mole fraction of the $Al_xGa_{1-x}N$ barrier layer of the three samples as 0.25, 0.23, and 0.22, respectively. [4]

To gain an understanding of the sample surface quality (cracks and defects), several investigations were conducted. Figure 3 shows the optical microscopy (OM), AFM and CL images of samples A, B and C. Optical microscopy reveals no surface cracks. AFM reveals similar average root-mean-square (RMS) roughness of sample A (5.5 ± 2.8 Å), B (5.2 ± 1.4 Å), and C (5.1 ± 1.3 Å). In addition, AFM and cathodoluminescence (CL) studies are conducted to reveal defectivity of samples A, B, and C (Table I). XRD rocking curve scan on (002) and (102) planes are also performed to highlight the screw-type and edge-type threading dislocation densities, based on the FWHM (i.e. $\beta_{(002)}$ and $\beta_{(102)}$) of the measured peaks (Fig. 4) and the estimation equation below:

$$D_{\mathrm{screw}} = \frac{\beta_{(002)}^2}{4.35 b_{\mathrm{screw}}^2},$$

$$D_{\mathrm{edge}} = \frac{\beta_{(102)}^2 - \beta_{(002)}^2}{4.35 b_{\mathrm{edge}}^2},$$

where the screw-type Burgers vector length (b_{screw}) is 0.5185 nm and the edge-type Burgers vector length (b_{edge}) is 0.3189 nm. The results of the defectivity investigation are tabulated in Table I. AFM and CL studies agree that sample A (with a 6.3 µm epi thickness) has the lowest threading dislocation density, whereas the AFM study reveals that sample C (with 1.1 µm epi thickness) has the highest one, indicating the effect of buffer layers on reducing threading dislocations, because of the higher probability of merging and canceling between threading dislocations. Since a CL investigation tends to underestimate defectivity due to multiple threading dislocations locating within one capture radius, the AFM defectivity is assumed to be the total defectivity. We therefore conclude that, except for the screw- and edge-type, sample C possesses a large amount of other kinds of surface defects.

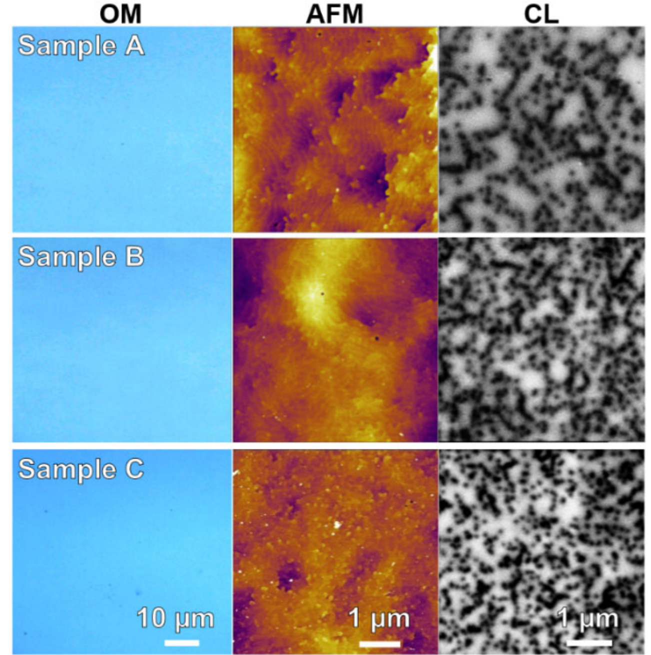

Fig. 3. Optical microscopy (first column), AFM (second column), CL panchromatic images (third column) of sample A, B, and C. [4]

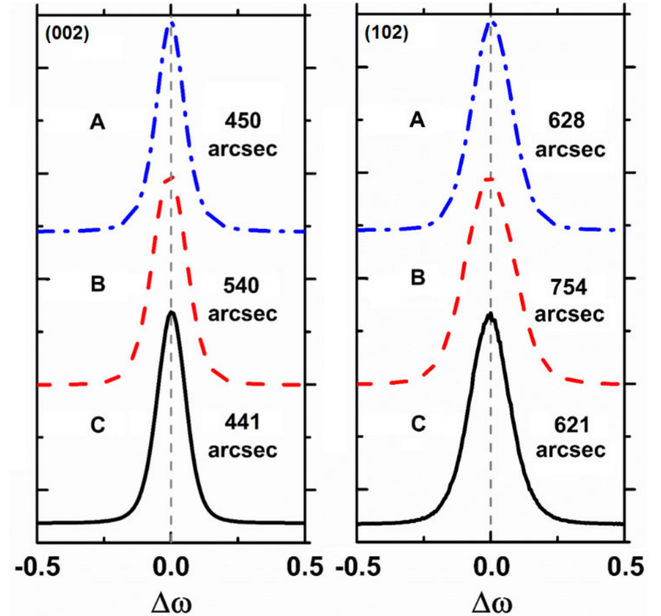

Fig. 4. XRD omega (rocking curve) scans on (002) and (102) plans for respectively estimating the densities of screw- and edge-type threading dislocations in samples A, B, and C. [4]

TABLE I.
AFM, CL, AND XRD SURFACE DEFECTIVITY. [4]

($\times 10^9$ cm^{-2})	Sample A	Sample B	Sample C
AFM	1.8	2.2	2.6
CL	1.0	2.0	1.8
XRD	Screw: 0.40 Edge: 1.02	Screw: 0.58 Edge: 1.47	Screw: 0.39 Edge: 1.02

XRD reciprocal space mapping was conducted on (002) and (105) planes to accurately reveal the Al composition (x) of all the graded $Al_xGa_{1-x}N$ buffer layers (sample A: $Al_{0.33}Ga_{0.67}N$ / $Al_{0.60}Ga_{0.40}N$ / $Al_{0.82}Ga_{0.18}N$; sample B: $Al_{0.30}Ga_{0.70}N$ / $Al_{0.58}Ga_{0.42}N$ / $Al_{0.82}Ga_{0.18}N$) and the in-plane strain of each layer based on the equation:

$$\left(\frac{1}{d_{\mathrm{hkl}}}\right)^2 = \frac{4}{3}\left(\frac{h^2+hk+k^2}{a_{\mathrm{m}}^2}\right)+\frac{l^2}{c_{\mathrm{m}}^2},$$

and the Poisson-Vegard's law [5]:

$$\begin{cases} \dfrac{c_m(x)-c_0(x)}{c_0(x)} = -\dfrac{2v(x)}{1-v(x)} \times \dfrac{a_m(x)-a_0(x)}{a_0(x)} \\ c_0(x) = xc_{\mathrm{AlN}} + (1-x)c_{\mathrm{GaN}} + \delta_{\mathrm{c}} \cdot x \cdot (1-x) \\ a_0(x) = xa_{\mathrm{AlN}} + (1-x)a_{\mathrm{GaN}} + \delta_{\mathrm{a}} \cdot x \cdot (1-x) \\ v_0(x) = xv_{\mathrm{AlN}} + (1-x)v_{\mathrm{GaN}}, \end{cases}$$

where d_{hkl} represents the measured interplanar spacing of the probed lattice plane (*hkl*); a_{m} and c_{m} are the calculated lattice constants. The Poisson ratio v_{AlN} and v_{GaN} are 0.203 and 0.183, respectively. δ_{c} and δ_{a} represent the deviation (bowing) parameter equal to -0.036 and 0.018 Å, respectively. In addition, in-plane strain (σ_{xx}) can be further calculated based on the in-plane stress (ε_{xx}) via equations:

$$\varepsilon_{xx} = \left[a_{\mathrm{m}}(x) - a_0(x)\right] / a_0(x),$$
$$\sigma_{xx} = \left[(C_{11}+C_{12}) - 2C_{13}{}^2 / C_{33}\right] \times \varepsilon_{xx},$$

where C_{ij} are the elastic constants of GaN (C_{11} = 390 GPa, C_{12} = 145 GPa, C_{13} = 106 GPa, and C_{33} = 398 GPa). As shown in Fig. 5, the GaN layers of samples (A, B, C) are all under tensile strain along the c-plane (1.059, 0.154, and 1.548 GPa for GaN in sample A, B, and C, respectively). For samples A and B, the in-plane strain first decreases from positive (tensile), crossing the zero line (strain-free), and then become negative (compressive) from the AlN layer toward the $Al_xGa_{1-x}N$ layers. Finally, due to the growing of the GaN layer, the layer in-plane strain returns to positive (tensile). Of our samples, sample B is measured to have the lowest GaN in-plane tensile stress due to its graded $Al_xGa_{1-x}N$ buffer layers. Surprisingly, sample A has a larger GaN in-plane tensile strain than sample B; we attribute this to the fact that sample A has carbon dopants that potentially limit the movement of dislocations while growing, which further limits the dislocation reduction and the relief of the GaN tensile stress. On the other hand, without any $Al_xGa_{1-x}N$ buffer layer, the GaN in-plane tensile strain of sample C is the highest.

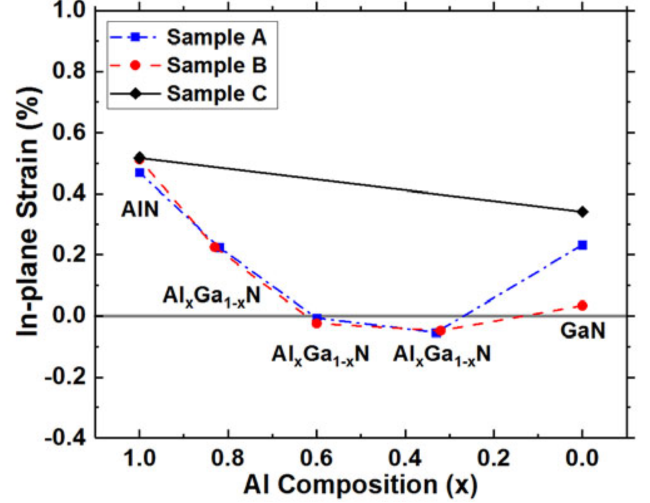

Fig. 5. In-plane strain of AlN, $Al_xGa_{1-x}N$, and GaN of sample A, B, and C obtained from XRD RSM study (symmetric (002) plane and asymmetric (105) plane). [4]

Samples with Van der Pauw configuration were prepared for Hall measurements: 5 mm × 5 mm square samples were deposited with 200-nm-thick Ti / 200-nm-thick Ni in the four corners and then annealed at 750 °C under N_2 for 45 seconds in order to form ohmic contacts. Hall measurements were conducted at room temperature (RT) and 77 K using multiple prepared samples, and the averaged results are shown in Table II. Sample B possesses the lowest 2DEG concentration and the highest 2DEG mobility [4]. At low temperature (77K), the 2DEG mobility increases and the sheet resistance decreases in all samples due to the reduced phonon scattering at low temperature. Furthermore, 2DEG concentrations in all our samples are higher at 77 K than at 300K.

TABLE II.
HALL MEASUREMENT RESULTS OF SAMPLE A, B, AND C.

	R_s (Ω/□)		2DEG N_s (10^{13} cm^{-2})		2DEG μ_n (cm^2/V-s)	
	RT	77 K	RT	77 K	RT	77 K
A	431.8	110.8	1.20	1.30	1295	4867
B	385.8	66.5	0.89	1.00	1802	9175
C	445.5	96.0	0.92	1.00	1593	6930

DISCUSSION

The defectivity measurements via AFM and CL reveal that the density of threading dislocations can be reduced if the material is grown with a thicker total buffer layer. We further show that step-graded $Al_xGa_{1-x}N$ buffer layers and

thicker GaN buffer layers alone are beneficial in doing so. This is due to an increase of the interaction of edge- and mixed-type threading dislocations in the form of fusion and annihilation. Inaccuracy of CL investigation, as mentioned, is due to multiple threading dislocations locating within one capture radius. On the other hand, the inaccuracy of XRD defectivity can be attributed to the fact that the measured XRD rocking curve FWHM is not solely affected by threading dislocations; other influences such as micro-strain, wafer curvature and instrumental broadening can also alter the FWHM. Therefore, AFM defectivity is then suggested to be considered as the total defectivity.

X-ray diffraction RSM was used to investigate strain distribution in the buffer layers; it can provide in-/out-of-plane strain information of GaN, $Al_xGa_{1-x}N$, and AlN layers. In samples A, B and C, the AlN in-plane tensile strains were 0.47%, 0.51%, and 0.52%, respectively. A gradual reduction of in-plane tensile strain was observed in the step-graded 3 × $\{Al_xGa_{1-x}N\}$ buffer layers. This leads to a lower tensile GaN in-plane strain in samples A (0.23%) and B (0.03%) than that in sample C (0.34%), showing the importance of employing step-graded buffer layers.

Hall measurement revealed that sheet resistance is inversely related to the 2DEG mobility; in addition, a trade-off between the 2DEG concentration and 2DEG mobility can also be seen. Based on the fact that sample A has the lowest threading dislocations but sample B has the lowest in-plane strain and the highest 2DEG mobility, our work suggests that 2DEG mobility is not solely affected by threading dislocations but also by GaN in-plane strain. The concentration of 2DEG depends on the spontaneous (P_{SP}) and piezoelectric (P_{PE}) polarizations in the $Al_xGa_{1-x}N$ barrier layer and the underlying GaN layer, as described by equation:

$$\sigma\left(P_{\mathrm{SP}}+P_{\mathrm{PE}}\right)=P(\mathrm{GaN})-P(\mathrm{Al}_x\mathrm{Ga}_{1-x}\mathrm{N})$$
$$=\left\{P_{\mathrm{PE}}\left(\mathrm{GaN}\right)-P_{\mathrm{PE}}\left(\mathrm{Al}_x\mathrm{Ga}_{1-x}\mathrm{N}\right)\right\}$$
$$+\left\{P_{\mathrm{SP}}\left(\mathrm{GaN}\right)-P_{\mathrm{SP}}\left(\mathrm{Al}_x\mathrm{Ga}_{1-x}\mathrm{N}\right)\right\},$$

where P_{SP} is independent of strain. P_{PE} can be further described as:

$$P_{PE}=2\frac{a-a_0}{a_0}\left(e_{31}-e_{33}\frac{C_{13}}{C_{33}}\right).$$

where C_{13} and C_{33} are elastic constants and e_{31} and e_{33} are piezoelectric coefficients. Since the $Al_xGa_{1-x}N$ barrier layer is thin (~ 17 nm), we can fairly assume that there is no relaxation of the AlGaN barrier layer on top of the GaN layer, meaning that they should have the same lattice constant *a*. It can be calculated that a larger GaN in-plane tensile strain can lead to a larger in-plane AlGaN barrier; given the difference between the elastic constants and the piezoelectric constants of GaN and $Al_xGa_{1-x}N$, the simultaneous increase of the strain of the second layer enhances the piezoelectric polarization, which further increases the 2DEG concentration.

Carrier-concentration-dependent 2DEG mobility was investigated by O. Katz *et al.* [6]. At different concentrations of 2DEG concentration, different scattering mechanisms dominate the 2DEG mobility. When the 2DEG concentration is high (> 2×10^{12} cm^{-2}), an effect caused by the interface roughness scattering that downgrades the 2DEG mobility was observed and explained. With an increase of the 2DEG concentration, the ground state wave function in the quantum well actually shifts towards the side of the interface, which is also in line with the fact that a stronger polarization can induce more 2DEG in the triangular quantum well, and also attract the electrons to populate closer to the interface. Hence, with a higher 2DEG concentration the interface roughness can cause more severe electron scattering, which leads to a lower 2DEG mobility. In our work, sample B has the lowest in-plane GaN tensile strain, leading to its low 2DEG concentration. The low 2DEG concentration reduces the interface roughness scattering, therefore the 2DEG mobility of sample B surpasses the other two samples.

CONCLUSIONS

It is shown that 2DEG characteristics are heavily affected by the buffer layers grown between the AlGaN/GaN HEMT structures and the Si(111) substrates. Particularly, we report that in-plane stress in the GaN layer, not the surface defectivity, dominates the 2DEG characteristics: a lower GaN in-plane stress reduces the 2DEG concentration (due to the less piezoelectric polarization), which further increases the 2DEG mobility (due to the less 2DEG channel interface roughness scattering) [4]. Buffer layer engineering is shown to be essential for achieving high 2DEG mobility (> 1800 cm^2/V·s) and 2DEG carrier concentration (> 1.0×10^{13} cm^{-2}) on 200-mm-diameter Si(111) substrates.

ACKNOWLEDGEMENTS

This work was partially supported by the Air Force Office of Scientific Research (AFOSR) through Young Investigator Program Grant FA9550-16-1-0224 and was carried out in the Micro and Nanotechnology Laboratory and Frederick Seitz Materials Research Laboratory Central Facilities, University of Illinois at Urbana-Champaign, IL, USA.

REFERENCES

[1] M. Ishida, *et al.*, *IEEE Trans. Electron Dev.* **60**, 3053 (2013).
[2] A. Able, *et al.*, *J. Cryst. Growth.* **276**, 415 (2005).
[3] J. Perozek. *et al.*, *J. Phys. D: Appl. Phys.* **50**, 055103 (2017).

[4] H.-P. Lee, *et al.*, *Sci. Rep.* **6**, 37588 (2016).
[5] A. Kadir, *et al.*, *Appl. Phys. Lett.* **105**, 232113 (2014).
[6] O. Katz, *et al.*, *IEEE Trans. Electron Dev.* **50**, 2002 (2003)

ACRONYMS

HEMT: high electron mobility transistor
2DEG: 2-dimensional electron gas
AFM: atomic force microscopy
CL: cathodoluminescence
XRD: X-ray diffraction
RSM: reciprocal space mapping
FWHM: full width half maximum